PRESTACK SEISMIC DATA ENHANCEMENT WITH PARTIAL COMMON REFLECTION SURFACE (CRS) STACK

M. Baykulov and D. Gajewski

email: *mikhail.baykulov@zmaw.de*

keywords: *Common Reflection Surface (CRS) stack, partial CRS stack, regularisation*

ABSTRACT

A partial Common Reflection Surface (CRS) stacking method is developed to enhance the quality of sparse low fold seismic data. Kinematic wavefield attributes computed during the automatic CRS stack are used to enhance the prestack data. A multi-parameter CRS traveltime formula is used to compute partial stacked CRS supergathers. We developed an algorithm, which allows to generate NMO-uncorrected gathers without the application of inverse NMO/DMO. Gathers obtained by this new approach are regularised and have better signal-to-noise ratio compared to original common-midpoint gathers. Instead of the original data, these improved prestack data can be used in many conventional processing steps, e.g., velocity analysis or prestack depth migration, providing enhanced images and better quality control. We verified the method on 2D synthetic data and applied it to low fold land data from Northern Germany. The synthetic examples show the robustness of the partial CRS stack in the presence of noise. Sparse land data were regularised, and the signal-to-noise ratio of the seismograms was increased as a result of the partial CRS stack. Prestack depth migration of the generated partially stacked CRS supergathers produced significantly improved common-image gathers as well as depth migrated sections.

INTRODUCTION

The quality of reflection seismic data is very important for seismic processing. It depends on a number of factors, e.g., the topography of the Earth surface, the complexity of the subsurface, and the technical equipment used in the acquisition stage. The presence of natural and anthropogenic factors can also affect land seismic measurements (see, e.g., Stolt, 2002; Spitzer et al., 2003; Chandola et al., 2004). Inhomogeneities in the subsurface, the presence of fault structures and strong velocity contrasts like in the areas of salt plugs lead to a decrease of the signal-to-noise ratio (S/N) of the data.

Quite often the quality of old seismic reflection data, which needs to be reprocessed, is comparably low, because of the short maximum offsets, irregular acquisition, and low CMP fold. All these factors lead to a more complicated workflow to precondition the data for velocity analysis, velocity model building and other processes. The quality of time and depth migrated stacked sections is consequently poor. The prestack common midpoint (CMP) gathers of real land data may contain sparse seismograms located irregularly over the short offset range. Regularisation of seismograms and filling the gaps in case of missing data is usually performed using different binning and interpolation techniques (see, e.g., Brune et al., 1994; Yilmaz, 2001; Stolt, 2002; Fomel, 2003; Spitzer et al., 2003; Chandola et al., 2004; Herrmann et al., 2008).

The *Common Reflection Surface* (CRS) stack technology based on multi-parameter stacking (see, e.g., Müller, 1999; Jäger et al., 2001; Mann, 2002) was already successfully applied by Yoon et al. (2008) and Baykulov et al. (2008) to enhance the time sections of old low fold seismic reflection data from Northern Germany. In this paper we show the possibility of the CRS stack method to improve the quality of 2D prestack data. The CRS traveltime formula, where the dip of the reflector element is incorporated, is used to compute new partially stacked CRS supergathers, where each trace is a result of summation of data

along the CRS stacking surface. The number and location of traces in the produced supergathers can be defined, e.g., to fill areas of missing offsets. Since no interpolation, but a summation of data is performed, the method is very robust in the presence of non-coherent noise. Moreover, the regularisation of traces can be performed with the partial CRS stack. The CRS stacking surface approximates the traveltimes of seismic reflection data more precisely than the NMO/DMO stack (see, e.g., Müller, 1999; Jäger et al., 2001). Therefore, the application of the CRS stacking surface to produce regularised data can be superior to the methods based on the conventional NMO/DMO and binning/interpolation techniques described by Brune et al. (1994).

THEORY

CRS stacking surface

The CRS stack is a multi-parameter stacking technique. The CRS stacking surface (see Figure 1) results from approximating the true subsurface reflector by a reflector element that locally has the same curvature as the true reflector. The traveltime t of reflection events is described by three parameters α, R_n and R_{nip} in a hyperbolic formula:

$$t^2(m,h) = \Big(t_0 + \frac{2sin\alpha}{V_0}m\Big)^2 + \frac{2t_0cos^2\alpha}{V_0}\Big(\frac{m^2}{R_n} + \frac{h^2}{R_{nip}}\Big), \tag{1}$$

where h is half source-receiver offset, m is the midpoint displacement with respect to the considered CMP position, and t_0 corresponds to the zero offset (ZO) two-way traveltime (TWT). In equation 1 α is the angle of emergence of the ZO ray, V_0 is the near surface velocity, R_n and R_{nip} are radii of curvature of the normal (N) wave and normal-incidence-point (NIP) wave, respectively. The N- and NIP-waves are generated by two hypothetical one-way experiments (see Hubral, 1983). R_{nip} can be associated with the distance from the reflector element to the observation surface, and R_n is a measure for the CRS's curvature. However, the exact position of the reflector element can be defined only after performing a seismic inversion procedure, e.g. the NIP-wave tomography, as implemented by Duveneck (2004). In the following the parameter triplets (α, R_n and R_{nip}) are referred to as the *CRS parameters*.

Depending on the maximum CMP displacement m, the CRS stacking surface (green grid in Figure 1) contains a number of traces larger than the number used during the conventional CMP stack (magenta line in Figure 1). The choice of the maximum midpoint displacement m is important for the resulting lateral resolution of the following processing results. The size of the first projected Fresnel zone is a good guidance for this parameter which can be interpreted as the lateral extension of the stacking operator. However, the CMP stack can be considered as a special case of the CRS stack with the maximum midpoint displacement $m = 0$. In that case, the equation 1 transforms into the classical CMP stacking formula:

$$t^2(h) = t_0^2 + \frac{4h^2}{V_{nmo}^2}, \tag{2}$$

where $V_{nmo} = \sqrt{\frac{2VoRnip}{t_0cos^2\alpha}}$ is the stacking velocity.

Partial CRS stack

Partial CRS stack calculates a stacking surface around a specified point defined by its offset and traveltime coordinates in a chosen CMP location, and performs the summation of data along that surface. The result of summation is assigned to a new sample with the same CMP, offset, and time coordinates. Repeating this procedure for all desired points generates a new gather that is called *(partially stacked) CRS supergather* in the following. In Figure 1 the partial CRS stack surface is shown as a red grid around the specified event (red point) in a chosen CMP gather. That surface coincides locally with the CRS stack surface shown as a green grid, but the size of the partial CRS stacking surface is smaller than that of the CRS stack surface.

The partial CRS stacking surface is defined by the zero-offset (t_0) time of the considered point and the corresponding CRS parameters. The size of the surface may vary from the size of the CRS stack surface described in the previous section. Although it may be a good choice to use the same size of the surface as it is used for the CRS stack, the maximum offset or midpoint displacement from the chosen point

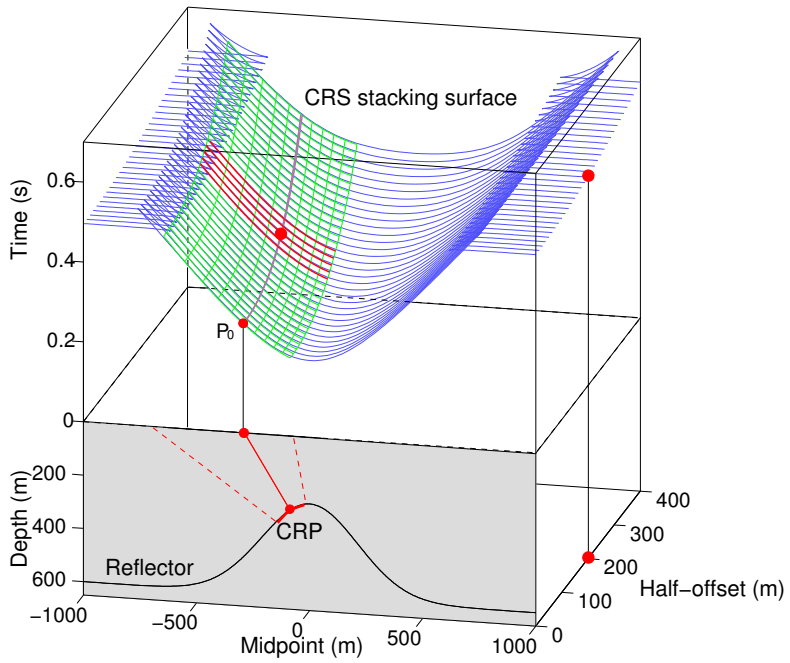

Figure 1: CRS stacking surface for a constant velocity medium. The CRS stack sums the data along the green surface and assigns the result to the point P_0. The stacking surface results from approximating the true subsurface reflector by a reflector segment that locally has the same curvature as the true reflector. The partial CRS stack performs the summation of data around the specified point on a CMP traveltime curve (magenta line), and assigns the result to that point in a new generated CRS supergather. The partial CRS stacking surface shown with a red colour coincides locally with the CRS stacking surface, but may be limited in size (in this case only five neighbouring offsets and full midpoint range are considered to generate one trace in the CRS supergather)

may be smaller than that defined for the CRS stack surface. The measurements of the partial CRS stack surface in offset and midpoint dimensions are called *partial CRS stack apertures* in the following. These apertures should be adjusted according to the aim of processing, and may enclose only some traces on the CRS stacking surface around the chosen point. Stacking more traces may be necessary to fill large data gaps present in the CMP gathers. In that case the information from the neighbouring CMPs or from the neighbouring offsets is used to generate a new trace in the CRS supergather.

Since the partial CRS stack performs the summation of data to generate one sample in the CRS supergather, it enhances the quality of the seismograms by increasing their S/N ratio. Moreover, taking information from the neighbouring traces into account allows to fill data gaps. Finally, the CRS stacking surface can be calculated for every desired offset, which means that the data regularisation within each gather can be performed. The incorporation of the midpoint displacement m into the calculation of the partial CRS stacking surface results in the construction of CRS supergathers, where the dip of reflectors is taken into account. Due to this the partial CRS stack method is superior to the conventional CMP binning technique (see, e.g., Yilmaz, 2001), where the dip of the structure is not considered. As it is shown in Müller (1999) and Jäger et al. (2001), the CRS stacking surface better describes the reflection response compared to the NMO/DMO stack. Therefore, the partial CRS stack should produce better results than the existing NMO/DMO interpolation schemes as described by Brune et al. (1994). Only for the rare case when the shape of the true subsurface reflector is identical to the shape of the specific ZO isochrone, the NMO/DMO stacking surface describes the data identical to the partial CRS stacking surface (see, e.g., Jäger et al., 2001).

Since the partial CRS stacking surface is calculated not only for the zero-offset trace, but for every specified source-receiver offset, and the result of partial stacking is assigned to the trace with the specified

offset, the output gathers are not NMO-corrected. Therefore, the partial CRS stack supergathers may further be used in many standard precessing steps like velocity analysis, stacking, or migration.

Calculation of partial CRS stacking surface

The partial CRS stacking surface is calculated in a chosen CMP location for every specified sample $A(t_A, h_A)$, where t_A is two-way traveltime, and h_A is half source-receiver offset. The accurate zero-offset time, and the corresponding CRS parameters (α, R_n, R_{nip}), describing this event, need be found. We developed a search algorithm optimized to find at offset h_A zero-offset traveltime of the partial CRS stacking surface that exactly fits the sample A. The CRS parameters for each CMP location in the stacked volume must be known. These CRS parameters are determined by the automatic search described by Müller (1999), Jäger et al. (2001) and Mann (2002).

The zero-offset traveltime search is performed for every CMP location of the data independently. Since the CMP traveltime curve is a special case of the CRS stack surface when the midpoint displacement $m = 0$ (see equation 2), this search is simplified to find the CMP hyperbola that best fits the event in A. All zero-offset traveltimes within the range $[0; t_A]$ and the corresponding CRS parameters are tested to determine the hyperbola that has the minimum time deviation from t_A at the offset h_A. Following from the equation 2 the traveltime of best-fitting CMP curve is described as

$$t^2(h) = t_0'^2 + \frac{2t_0' cos^2\alpha}{V_0}\frac{h^2}{R_{nip}}, \tag{3}$$

where t_0' is the tested zero-offset traveltime, and α and R_{nip} are CRS parameters corresponding to that t_0'.

However, the defined hyperbola does not fit the event $A(t_A, h_A)$ exactly, because only discrete values of zero-offset traveltimes may be tested. The determined t_0', therefore, may not be used to describe the partial CRS stacking surface, because the events would not be stacked coherently in that case. Therefore, the CMP hyperbola has to be corrected to exactly fit the point A. Assuming that α and R_{nip} are changing smoothly around the considered event A, these parameters are fixed in the equation 3. Setting the traveltime t_A and the offset h_A of the event A into equation 3 yields

$$t_A^2 = t_0^2 + \frac{2t_0 cos^2\alpha}{V_0}\frac{h_A^2}{R_{nip}}, \tag{4}$$

where t_0 is a zero-offset traveltime of a CMP traveltime curve that fits the event A exactly. Solving this quadratic equation w.r.t. t_0 and neglecting the negative solution results in

$$t_0 = -\frac{h_A^2 cos^2\alpha}{V_0 R_{nip}} + \sqrt{\left(\frac{h_A^2 cos^2\alpha}{V_0 R_{nip}}\right)^2 + t_A^2}, \tag{5}$$

where α and R_{nip} are defined for the traveltime t_0'. Here we assume the R_{nip}, which is a measurement of a reflector depth, to be positive. Considering the negative values of R_{nip}, which may be useful for some special cases, it will be necessary to take the second solution of the equation 4 into account. The such defined t_0 is now used in the equation 1 to construct the partial CRS stacking surface that exactly fits the considered event A. This surface is used to sum up the data coherently.

RESULTS

In order to demonstrate the potential and advantages of the partial CRS stack method, we have applied it to the Sigsbee 2A synthetic dataset and a field dataset.

Noise free synthetic data

Sigsbee 2A is a constant density acoustic synthetic dataset released in 2001 by the "SMAART JV" consortium. Only a part of the dataset without the salt structure was used in this study. The data do not contain free surface multiples and almost no internal multiples due to very low acoustic impedance contrasts. Sigsbee 2A models the geologic setting found in the Sigsbee escarpment in the deep water Gulf of Mexico. A number of normal and thrust faults are present in the data. The source interval is 45.72 m. 348 channels per shot were used with a receiver spacing of 22.86 m. Therefore the resulting CMP interval is 11.43 m, and the maximum CMP fold is 87. The data were sampled every 8 ms with a total recording time of 12 s. In Figure 2(a) a typical CMP gather up to 3500 m offset and TWT=10 s is shown.

In total 500 CMP gathers were processed with the CRS stack method. First, the CRS parameters were found. The parameter estimation process is the most crucial part of the CRS stack processing. The simultaneous 3-parameter search would be computationally very expensive. We used three individual one-parametric search processes (automatic CMP stack, the angle scan, and the R_n scan) described in Müller (1999) and Jäger et al. (2001).

The CRS parameters were used to compute partial stacked CRS supergathers. The maximum midpoint displacement m was set up to 260 m at TWT=2.3 s and 900 m at TWT=11 s and interpolated linearly for intermediate values. The offset range of 914 m at TWT=2.3 s and 3810 m at TWT=11s was used and again interpolated linearly. The partial CRS stack aperture in offset dimension was limited to contain only one offset, which corresponds to the central common-offset red curve in Figure 1. The resulting CRS supergather is shown in Figure 2(b).

Although the source and receiver intervals of the Sigsbee 2A dataset are constant, the acquisition leads to a different sets of source-receiver offset in different CMP gathers. For example, only CMPs that are located directly in the positions of the sources contain zero-offset traces. As a result, only every fourth CMP has the same sets of offsets. Although it is not necessary to apply data regularisation for synthetic data, we adjusted the partial CRS stack such that the identical source-receiver offsets are present in the CRS supergathers. As a result, the CRS supergather has 4 times more traces than the CMP gather. The gathers are muted according to the defined offset aperture used during the CRS parameters search. Because of the larger number of traces, reflections in the CRS supergathers appear sharper and could be better distinguished in comparison to the CMP gather (see enlarged images in Figure 3).

CMP gathers and CRS supergathers were stacked with the same stacking velocity model obtained by the automatic CMP stack. Although it is possible to use the partial CRS stacked supergathers during the automatic CMP search to define a more reliable stacking velocity model, this is not shown in this paper in order to emphasize the improvement of the data quality only. Resulting ZO stacked sections are shown in Figure 4. The ZO CMP stack section (Figure 4(a)) displays a lower quality in the areas of fault structures and steep dipping layers. The CRS supergather stack (Figure 4(b)) shows better continuity of horizons at all time levels and produced a better image of conflicting dip areas. It is mentioned that conflicting dips areas are a problem to the CRS stack method. In case of crossing reflections only one dip is considered during the automatic parameter search with preference to the most coherent, i.e., strongest event. However, it is possible to analyse conflicting dips separately, which will result in a number of different CRS stack parameters (α, R_n, R_{nip}) for every point t_0 in conflicting dip areas. Although the partial CRS stack method takes the information about different conflicting dips into account, the automatic parameter search for Sigsbee 2A data was adjusted to consider only one dip. Therefore, the primary events were preferred, but the diffractions were attenuated as it is seen by comparing Figures 4(a) and 4(b). Nevertheless, we believe the stacked section of the CRS supergathers is clear, and is better suited for interpretation than the CMP stack section.

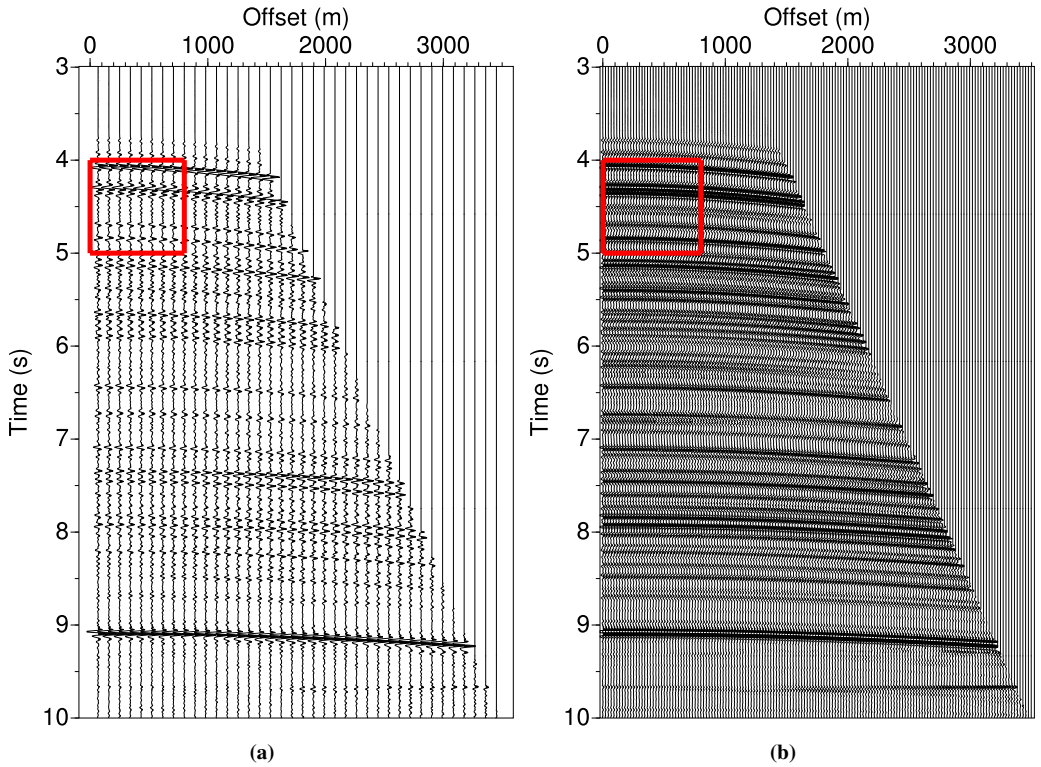

Figure 2: Noise free Sigsbee 2A data. Partially stacked CRS supergather (b) has 4 times more traces than the original CMP gather (a), providing better images of reflection events. The red rectangles are enlarged in Figure 3.

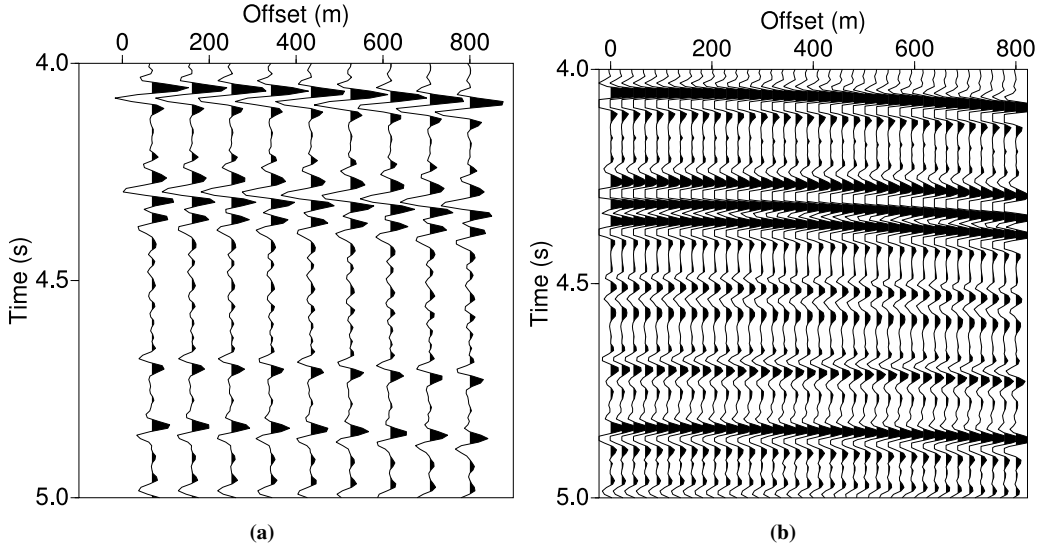

Figure 3: Enlargement of the noise free Sigsbee 2A data presented in Figure 2. The CMP gather (a) contains less traces than the partial stacked CRS supergather (b).

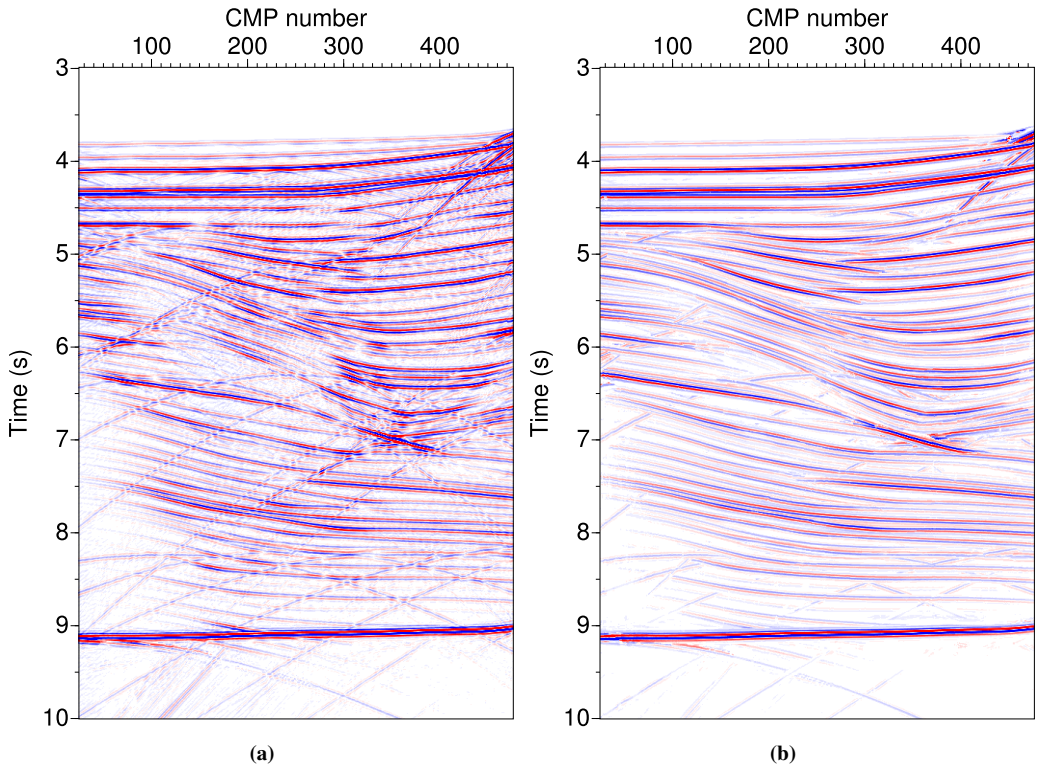

Figure 4: Noise free stacked Sigsbee 2A data. The conventional CMP stack (a) has lower quality in conflicting dips areas. In the CRS supergather stack (b) reflections are more continuous, and for conflicting dip areas appear clearer, and diffractions are attenuated.

Synthetic data with noise

To show the advantages of applying the CRS supergather method to noisy data, the direct waves were muted, and Gaussian noise with S/N=20 was added to the synthetic seismograms. The S/N ratio was computed w.r.t a signal with the maximum amplitude. As a result, only the strongest events like the reflection from the water bottom (4 s TWT) and the bottom of the model (9 s TWT) are visible in the CMP gather (Figure 5(a)). Since the amplitudes of all other reflections are lower, they are almost not visible. An automatic CRS parameter search was carried out for the noisy seismograms. Three one-parameter searches were performed in the same way as for the noise free dataset. The obtained CRS parameters were used to build the partial stacked CRS supergathers. The result is shown in Figure 5(b). Enlarged areas are shown in Figure 6. Compared to the CMP gather the reflections in the CRS supergather are clearly visible at all times. The noise is still present, but the S/N ratio is significantly increased.

Figure 7 demonstrates the advantage of CRS supergathers. Whereas the CMP stack of the noisy seismograms (Figure 7(a)) shows a lower S/N than the CMP stack in Figure 4(a), the stacked CRS supergathers (Figure 7(b)) have almost no visible differences compared to the stacked supergathers without noise (Figure 4(b)). This means, that the partial CRS stack is very stable to the presence of non-coherent noise. This advantage, however, requires a reliable determination of CRS parameters (α, R_n, R_{nip}).

Real land data

The CRS stack method was also applied to real data from Northern Germany. A part of a seismic reflection profile located north of the river Elbe and crossing the Jurassic salt plug in the Glückstadt Graben area was processed. The data were acquired in the 1980s using explosive sources with an average shot spacing of 120 m. For every shot gather 120 channels with a receiver spacing of 40 m were used. Irregular shooting geometry leads to a varying CMP fold with an average of 20. A typical example of a preprocessed CMP gather is shown in Figure 8(a). About 20 traces are located irregularly over the full offset range. Irregularity of traces accompanied by the low S/N leads to difficulties in identifying reflections both in the prestack gathers and in sections. Conventional binning of neighbouring CMP gathers into a new gather does not yield the desirable quality enhancement of the prestack data, because merging of data without the correction for the dip of the layers leads to smearing. Figure 8(b) shows a binned gather obtained by combining 10 CMP gathers, corresponding to a bin size of 200 m. The resulting CMP bin provides a better coherency of the reflection events in the upper part of the seismogram, but does not completely fill the gaps of data at certain offsets (around 2000 m and 3700 m). Combining 20 CMPs together (bin size 400 m) as shown in Figure 8(c) fills these gaps, but decreases the energy of reflection events. Combining more CMPs would further decrease the reflection coherency.

The automatic search of CRS parameters was performed to the dataset. We used the same approach as for the synthetic data, which is based on three one-parameter search processes. However, the stacking velocity model provided with the dataset was used as a guide to limit the range of estimated parameters. After the CRS parameters were estimated, partial stacked CRS supergathers were built. The maximum midpoint displacement during the partial CRS stack m was set up to 400 m at the surface and 2000 m at 5 s TWT and interpolated linearly for intermediate values. The offset range of 20 m at the surface and 4945 m at 5 s TWT was used and again interpolated linearly. Regularisation of traces was applied to the dataset with the partial CRS stack aperture in offset dimension adjusted to 100 m.

An example of a CRS supergather is shown in Figure 8(d). A significantly larger number of traces is present in the CRS supergather compared to the original CMP gather. The traces are well distributed, filling the gaps of the original CMP gather shown in Figure 8(a). Reflections are clearly visible at all times down to 4 s TWT. Also some events at TWT = 4.5-5 s, offset = 1000-2000 m are observed. Compared to the binned CMP gathers (Figure 8(b), Figure 8(c)), the CRS supergather provides a better S/N and a better continuity of reflections at all time levels. Partially CRS stacked data can be used in further conventional processing, e.g., for velocity analysis as well as for stacking and time or depth migration. Based on the depth migrated CRS supergathers residual moveout analysis and velocity model update can be performed.

Prestack Kirchhoff depth migration was applied to both CMP gathers and CRS supergathers. The migration velocity model was obtained by NIP-wave tomography inversion based on the CRS parameters (for details see Duveneck, 2004). In order to demonstrate the benefits of the partial CRS stack only, the

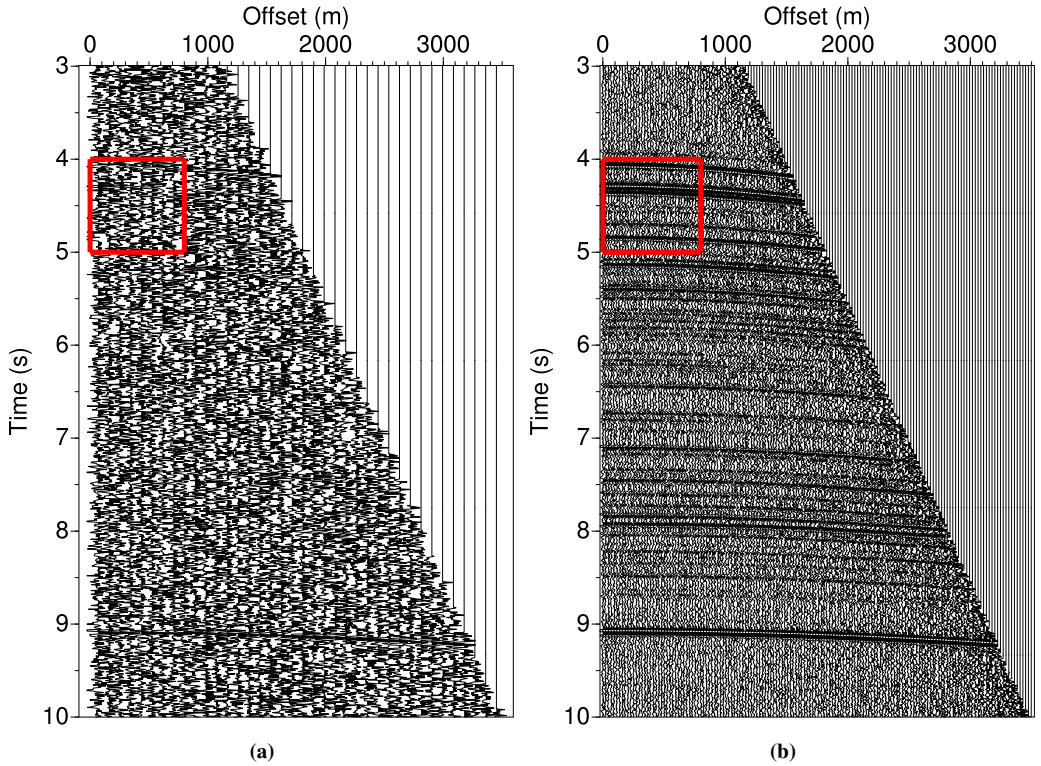

Figure 5: Sigsbee 2A data with noise. Reflections in the CMP gather (a) are hardly visible. The CRS supergather (b) displays a significantly increased S/N, and reflections are clearly visible from 4 to 9 s TWT. The red rectangles are enlarged in Figure 6.

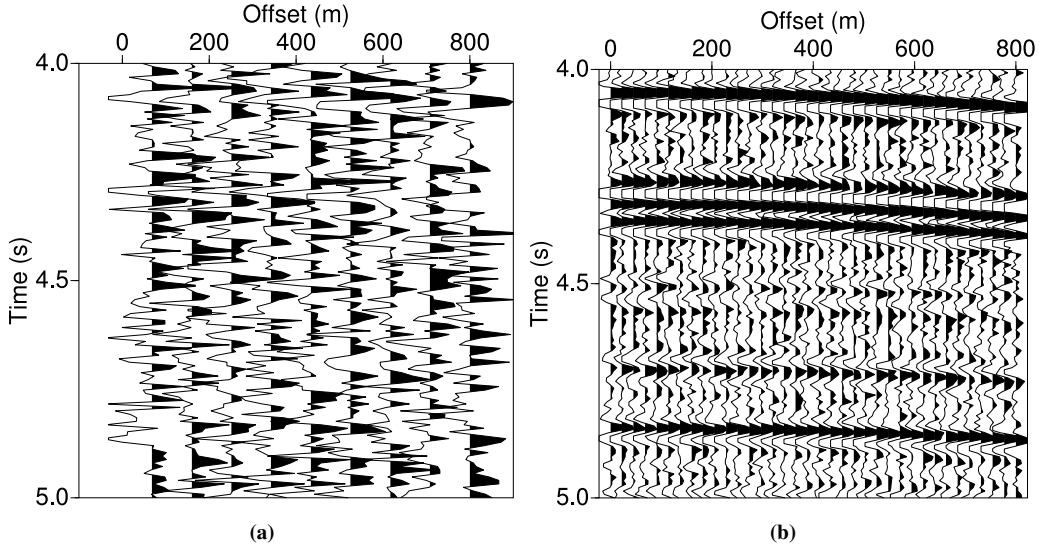

Figure 6: Enlargement of the Sigsbee 2A data with noise as presented in Figure 5. The CMP gather (a) contains less traces than the partial stacked CRS supergather (b). Reflections in the CMP gather can not be identified. The CRS supergather shows a significantly increased S/N. Several reflections are clearly visible.

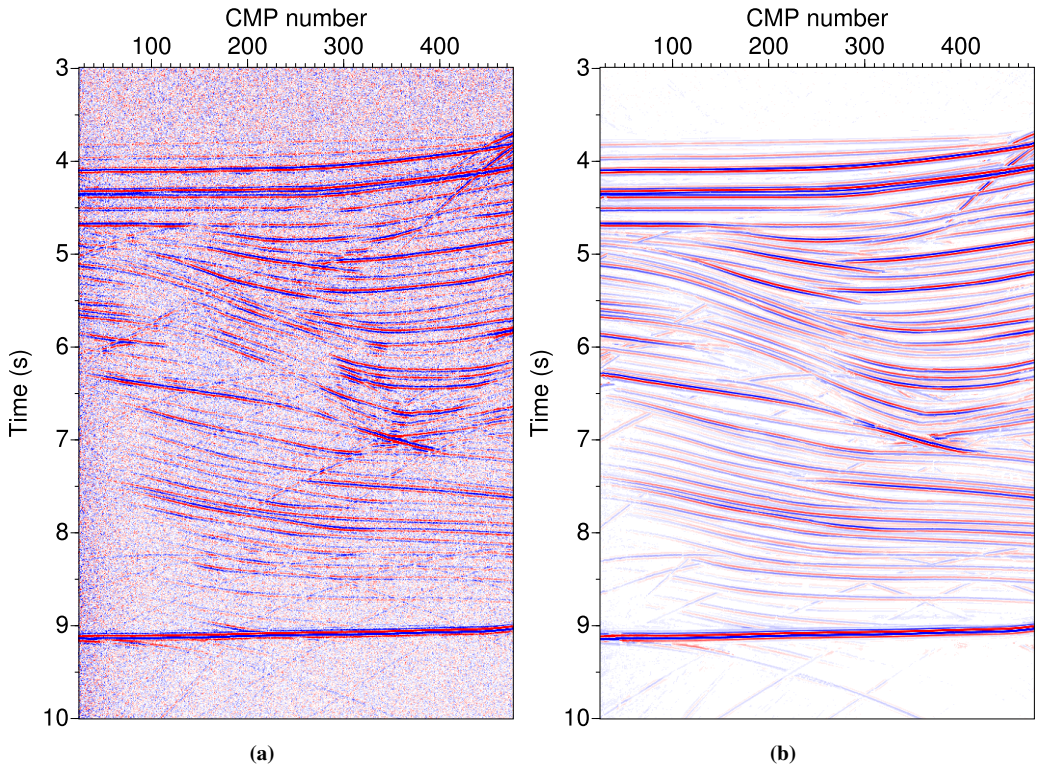

Figure 7: Stacked Sigsbee 2A data with noise. The conventional CMP stack has lower S/N compared to the CMP stack section without noise (Figure 4(a)). The CRS supergather stack shows almost no visual differences to the stacked section without noise (Figure 4(b)).

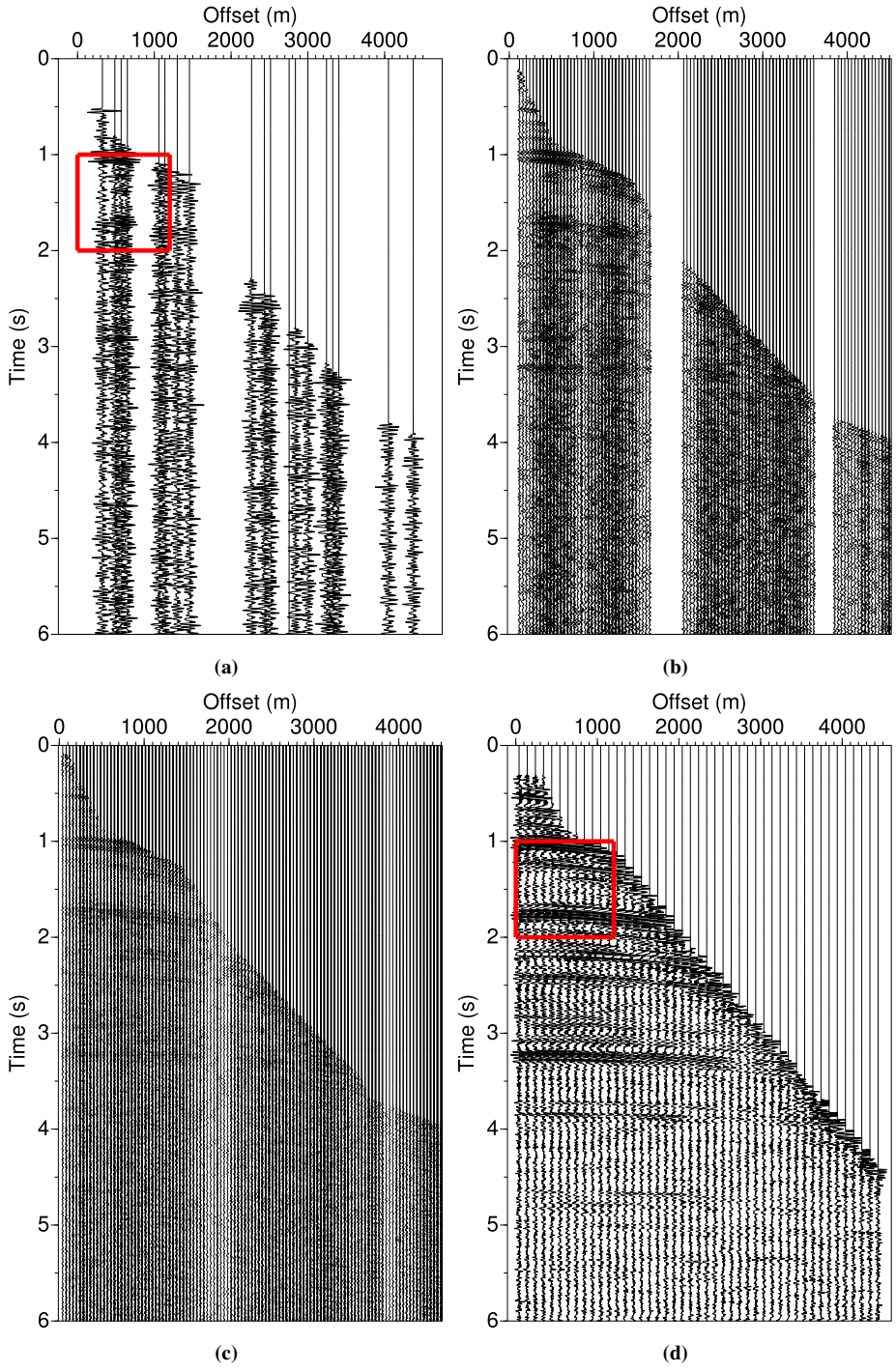

Figure 8: Real land data from Northern Germany. The CMP gather (a) has about 20 traces spaced irregularly. The CMP bins consisting of 10 CMPs (b) and 20 CMPs (c) increase the coherence of events, but does not improve the S/N. The CRS supergather (d) provides significantly increased S/N and better reflection continuity. The red rectangles are enlarged in Figure 9.

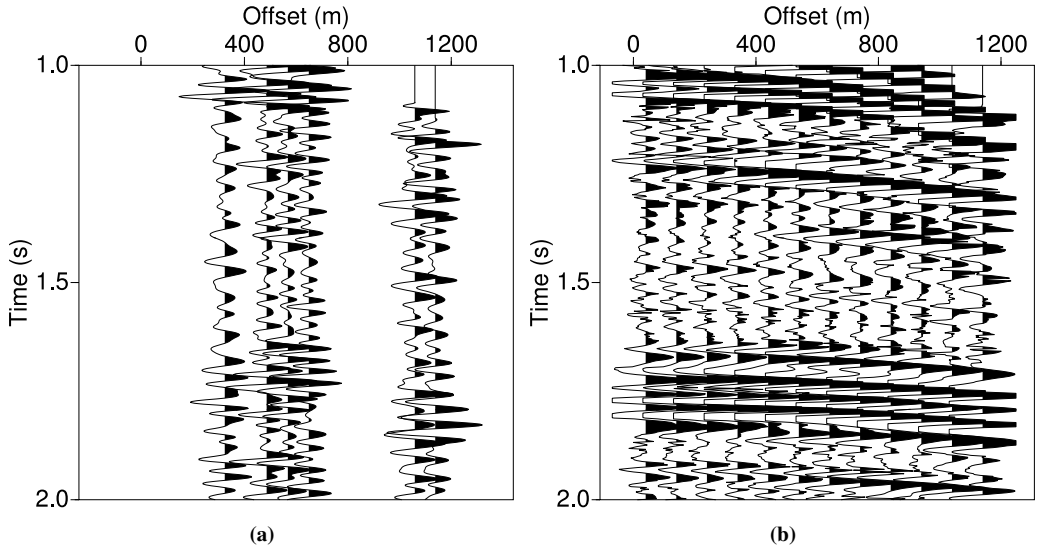

Figure 9: Enlargement of real land data from Northern Germany presented in Figure 8. The CMP gather (a) contains only a few traces spaced irregularly. Reflections are not visible, the S/N is low. The partial stacked CRS supergather (b) contains more traces with higher S/N than the CMP gather. The CRS supergather is regularised, and the data gaps present in the CMP gather are filled. Reflections are clearly visible and can be used for further processing steps like velocity analysis.

velocity model obtained for CRS parameters derived from the original CMP gathers was used to migrate both sets of original and partial stacked data. The improvement of the migration velocity model using the partial stacked CRS supergather for the NIP-wave tomography inversion may be the target of further investigations. The prestack Kirchhoff depth migration as applied here operates on common-offset gathers. Because of the irregular acquisition geometry, the original data were first preprocessed to build the binned common-offset gathers. Offset bin spacing was adjusted to the partial CRS stack offset aperture of 100 m. Performing a prestack depth migration (PreSDM) with the original data yields a depth-migrated section with low S/N shown in Figure 12. Prestack depth migrated common image gathers (CIG) shown in Figures 10(a) and 10(b) are only partially suited for residual moveout analysis and quality control. Only the strongest reflector at 1.2 km depth can be seen in Figure 10(a) and at 2, 4, 5, and 6 km depth in Figure 10(b).

PreSDM of the partially stacked CRS supergathers depicted in Figure 13 shows a significantly improved depth migrated section (compare to Figure 12). Horizons are more continuous, and a higher S/N is obvious. PreSDM of CRS supergathers provides better depth migrated gathers compared to the original CIGs (see Figures 10 and 11). Reflectors in the improved gathers are clearly visible and can be easily identified. The flat depth migrated CRS supergathers confirm the accuracy of the velocity model used for migration, which is hardly possible using the conventional CIGs. New depth migrated images of improved quality were used as a supplementary information for better interpretation, which provided an alternative view on the structural settings of the Glückstadt Graben area (Baykulov et al., 2008).

DISCUSSION

The partial CRS stack based on the CRS traveltime formula assumes the hyperbolic approximation of the reflection response. Therefore, the apertures of stacking in both offset and midpoint direction must be chosen carefully with respect to the complexity of the subsurface. However, the described search algorithm allows to find the best fit hyperbolic formula for the non-hyperbolic events as well. We suppose, that the robust summation in the midpoint direction used to generate the supergather would, nevertheless, produce reliable results also for non-hyperbolic. However, this point needs further investigations and may be the aim of the future work.

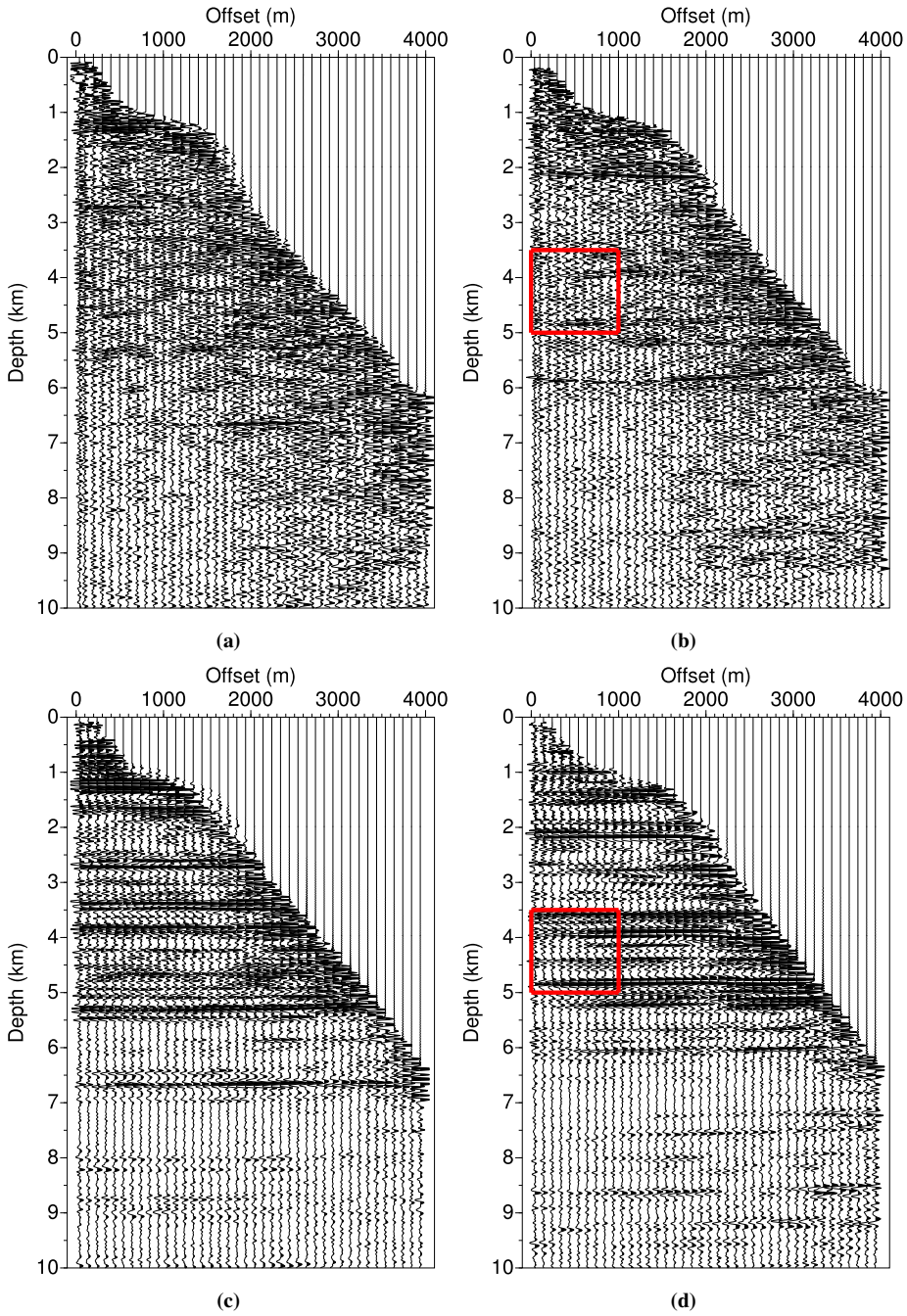

Figure 10: Prestack depth migrated CIGs of real land data located to the left and right of the salt plug (see Figure 12 and Figure 13). Conventional CIGs display only the strongest reflectors at 1.2 km depth for CIG 3100 (a) and at 2 to 6 km depth for CIG 2140 (b). The corresponding depth migrated CRS supergathers (c,d) have an increased S/N, and reflectors at levels down to 9-10 km depth are visible. The red rectangles are enlarged in Figure 11.

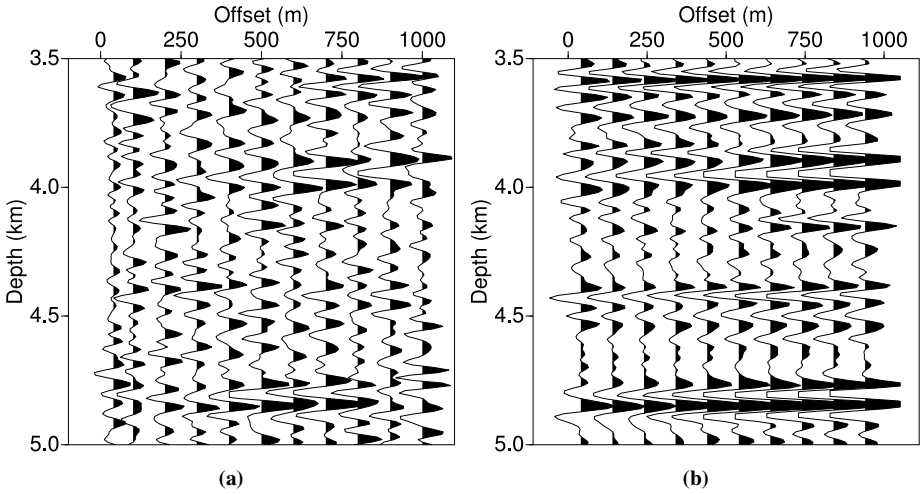

Figure 11: Enlargement of prestack depth migrated CIGs of real land data shown in Figure 10. The conventional CIG (a) is not suited to perform the residual velocity analysis and quality control, since the reflectors are hardly visible. The PreSDM of the partial stacked CRS supergather (b) shows much more continuous reflectors, which allows the further residual moveout analysis and quality control of the depth velocity model used in migration.

Since the partial CRS stack method performs summation of data, the true amplitudes are not preserved. However, by means of the CRS parameters it is possible to estimate the geometrical spreading factor required in true amplitude imaging. The application of the CRS stack for improved AVO analysis has already been presented by Pruessmann et al. (2004). Preservation of the true amplitudes in the partial stacks will be addressed in our future work efforts.

Here the method was implemented for the 2D case only. The first application of the 3D CRS stack on real 3D land data was presented by Bergler et al. (2002). They indicated some of the possible applications of the kinematic wavefront attributes estimated during the 3D CRS stack. Beyond the outlined applications, the partial CRS stacking surface can be computed for the 3D data as well, which is the aim of further investigations.

The partial CRS stack takes the information from conflicting dips into account, but to use this option the proper CRS parameters must be estimated. This results in a number of different stacking surfaces for one sample. The separated search for conflicting dips is already implemented in the 2D case.

Compared to the conventional CMP stack, the CRS stack requires more CPU time. For example, the automatic CMP stack of real land data used in this work took about 10 min, whereas the CRS stacking needed about 10 hours to complete where one CPU with 2.6 GHz and 1 GB RAM was used. More significant is the CPU time needed to estimate the CRS parameters, which took more than 10 days. The computation time, however, may vary depending on the apertures used by the CRS parameter search, the number of conflicting dips, and other factors. Much more difficult is to estimate the time that a user needs for testing the apertures, thresholds etc. Nevertheless, the CRS stack is an automatic approach that does not need any human intervention, when the processing parameters are known for the dataset. In this case the total time costs might be even less than the turnaround time of the conventional CMP processing. The partial CRS stack of the land dataset took about 30 hours to come up, which is quite fast compared to the CRS parameter search. It is important to mention that the CRS stack is an independent process for each sample and is well suited for parallelization. Using a computer cluster with a group of processors the computation time for the CRS parameter search and the partial CRS stack can be significantly reduced.

CONCLUSION

The presented partial CRS stack technique has shown the potential to enhance the quality of 2D prestack seismic data. Partial CRS stack generated new regularised gathers of higher quality. As a result of sum-

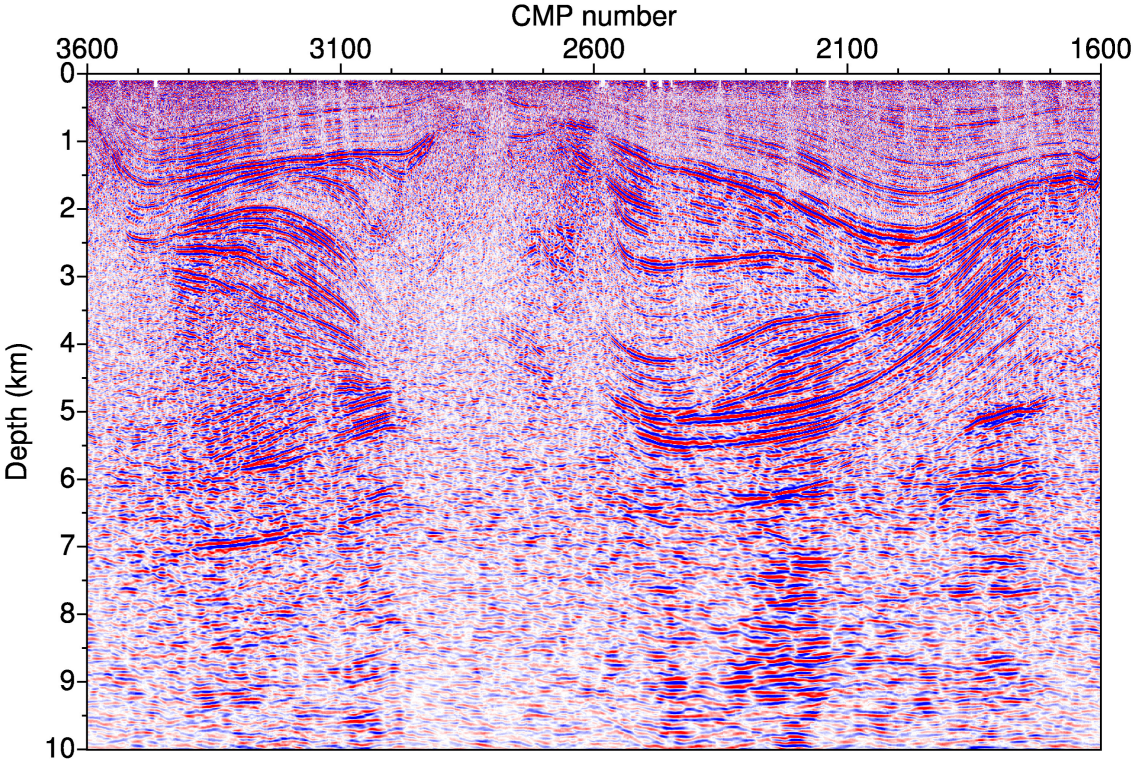

Figure 12: PreSDM section of CMP gathers. S/N is low. Reflectors are not continuous, the internal structure of the salt plug and the reflectors below 7 km depth are hardly visible.

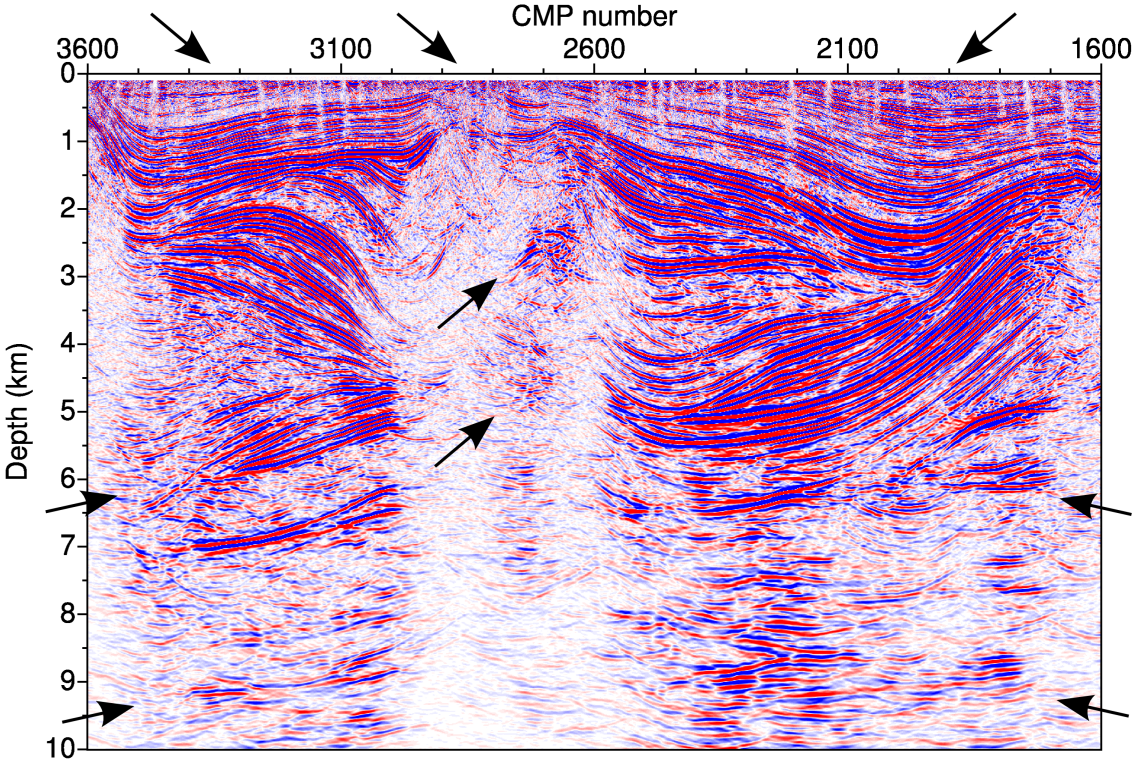

Figure 13: PreSDM section of CRS supergathers. The image quality is significantly enhanced compared to Figure 12. Horizons are more continuous, the enhanced S/N is obvious. Internal salt reflectors between 3000 and 2500 CMP at 2-6 km depth are identified. Also the image of the deeper part of the section below 7 km is improved. The areas of improvement are indicated by arrows.

mation, the S/N ratio of generated seismograms is higher compared to the original data. We successfully implemented the partial CRS stack method for the 2D case and applied it to synthetic data and to low fold land data from Northern Germany. Sparse land data were regularised, and the S/N of the seismograms was increased. Prestack depth migrated CRS supergathers of real data allowed a reliable quality control of the velocity model used for migration, which was not possible by conventional processing.

Our further work on this topic is the parallelization of the software and the application of the partial CRS stack on 3D data. Interpolation of data in missing CMP locations might be useful in the 3D case. Also the conflicting dip problem indicated in the discussion will be addressed in future work.

We recommend to use the partially stacked gathers instead of the conventional CMPs especially for sparse data of low quality. Results of velocity analysis, stacking and depth migration might be improved using the gathers generated by the new approach. Application to AVO analysis will be investigated, since the true amplitudes must be reconstructed. The optimised CRS parameter search can be carried out using the new gathers. The improved CRS parameter sets may further be used by the NIP-wave tomographic inversion. The CRS supergathers may also contribute to improve multiple attenuation.

ACKNOWLEDGEMENTS

We are grateful to the Wave Inversion Technology (WIT) consortium for supporting this project. The synthetic seismic data were produced by the Subsalt Multiples Attenuation and Reduction Technology Joint Venture (SMAART JV). The real land data were kindly provided by the WEG through the technical management of the German Society for Petroleum and Coal Science and Technology (DGMK). The processing of the data was partially supported through the grant Ga 350/12 of the priority program SPP 1135 of the German Research Foundation (DFG). We are thankful to Dr. Jürgen Mann for the fruitful discussions and suggestions for modifying the 2D CRS code. Discussions with Stefan Dümmong are appreciated.

REFERENCES

Baykulov, M., Brink, H.-J., Gajewski, D., and Yoon, M.-K. (2008). Revisiting the structural setting of the Glueckstadt Graben salt stock family, North German Basin. *Tectonophysics*. DOI:10.1016/j.tecto.2008.05.027.

Bergler, S., Hubral, P., Marchetti, P., Cristini, A., and Cardone, G. (2002). 3D common-reflection-surface stack and kinematic wavefield attributes. *The Leading Edge*, 21:1010–1015. DOI:10.1190/1.1518438.

Brune, R. H., O'Sullivan, B., and Lu, L. (1994). Comprehensive analysis of marine 3-D bin coverage. *The Leading Edge*, 13:757–762. DOI:10.1190/1.1437034.

Chandola, S. K., Singh, V., Saha, A., Sarma, P. L. N., Rao, M. P., and Ramakrishna, K. (2004). Seismic surveying in an urban setting. *The Leading Edge*, 23:1078–1082. DOI:10.1190/1.1813356.

Duveneck, E. (2004). Velocity model estimation with data-derived wavefront attributes. *Geophysics*, 69:265–274. DOI:10.1190/1.1649394.

Fomel, S. (2003). Seismic reflection data interpolation with differential offset and shot continuation. *Geophysics*, 68:733–744. DOI:10.1190/1.1567243.

Herrmann, F. J., Wang, D., Hennenfent, G., and Moghaddam, P. P. (2008). Curvelet-based seismic data processing: A multiscale and nonlinear approach. *Geophysics*, 73:A1–A5. DOI:10.1190/1.2799517s.

Hubral, P. (1983). Computing true amplitude reflections in a laterally inhomogeneous earth. *Geophysics*, 48:1051–1062. DOI:10.1190/1.1441528.

Jäger, R., Mann, J., Höcht, G., and Hubral, P. (2001). Common-reflection-surface stack: Image and attributes. *Geophysics*, 66:97–109. DOI:10.1190/1.1444927.

Mann, J. (2002). *Extensions and Applications of the Common-Reflection-Surface Stack Method*. PhD thesis, University of Karlsruhe.

Müller, T. (1999). *The Common Reflection Surface Stack Method: Seismic Imaging without explicit knowledge of the velocity model*. PhD thesis, University of Karlsruhe.

Pruessmann, J., Coman, R., Endres, H., and Trappe, H. (2004). Improved imaging and AVO analysis of a shallow gas reservoir by CRS. *The Leading Edge*, 23:915–918. DOI:10.1190/1.1803503.

Spitzer, R., Nitsche, F. O., Green, A. G., and Horstmeyer, H. (2003). Efficient acquisition, processing, and interpretation strategy for shallow 3D seismic surveying: A Case Study. *Geophysics*, 68:1792–1806. DOI:10.1190/1.1635032.

Stolt, R. H. (2002). Seismic data mapping and reconstruction. *Geophysics*, 67:890–908. DOI:10.1190/1.1484532.

Yilmaz, O. (2001). *Seismic data analysis - Processing, inversion, and interpretation of seismic data*. Soc. Expl. Geophys.

Yoon, M.-K., Baykulov, M., Duemmong, S., Brink, H.-J., and Gajewski, D. (2008). New insights into the crustal structure of the North German Basin from reprocessing of seismic reflection data using the Common Reflection Surface stack. *Int J Earth Sci*. DOI:10.1007/s00531-007-0252-5.